Static Equivalent Circuit Model for a Capacitive MEMS RF Switch

T. Tinttunen*, T. Veijola*, H. Nieminen**, V. Ermolov**, and T. Ryhänen**

* Department of Electrical and Communications Engineering
Helsinki University of Technology
P.O.Box 3000, FIN-02015 HUT, Finland. ttinttun@aplac.hut.fi
** Nokia Research Center, P.O. Box 407, FIN-00045 NOKIA GROUP, Finland

ABSTRACT

A simulation model for static analysis of a doubly supported capacitive MEMS RF switch has been constructed using electrical equivalencies. Energy-conserving large-displacement macro models for beam deflection, gap capacitance, electrostatic force, and mechanical contact are utilized. A one-dimensional finite-difference approach is utilized. The model is capable of reproducing the large-displacement beam deflection profile. The static model is verified by comparing APLAC® simulation results with measured CV characteristics. The results show that the model correctly reproduces the CV characteristics, including the performance at contact.

Keywords: MEMS, RF, Capacitive switch, Tunable capacitor, Equivalent circuit

1 INTRODUCTION

Micromechanical RF switches have challenged the traditional ways of controlling signals or power in a circuit. The switches are usually realized using a pin-diode or a FET. Capacitive switches have some advantages compared to semiconductor based switches. The lack of semiconductor p-n and metal-semiconductor junctions eliminates the contact and spreading resistances caused by ohmic contacts. Distortion and power levels are also better controlled since no nonlinearities caused by semiconductor junctions exist.

A capacitive micromechanical switch usually consists of two parallel plates. One plate is fixed and the other is suspended using mechanical springs in a way that a bias voltage can vary the gap between them. A simplified structure of a doubly supported capacitive switch is presented in Fig. 1. The switch operation is highly nonlinear and, typically for MEMS, energy is exchanged in several domains. The mechanical-domain beam deflection is produced with an electric-domain voltage. When the gap changes, a fluidic flow in the gas between the two surfaces occurs.

When designing a structure for a capacitive switch, the critical parameters are the on/off capacitance ratio, as well as the actuation voltage values that will change the switch state. The need for a simulation model that can reproduce these key issues is apparent. Some models have been presented for a doubly supported switch, e.g., in [1], [2].

2 CAPACITIVE SWITCH MODEL

When formulating a model for static features, the switch operation can be divided into three parts; beam deflection profile, capacitance and electrostatic force, and mechanical contact. Combining these parts forms the complete model.

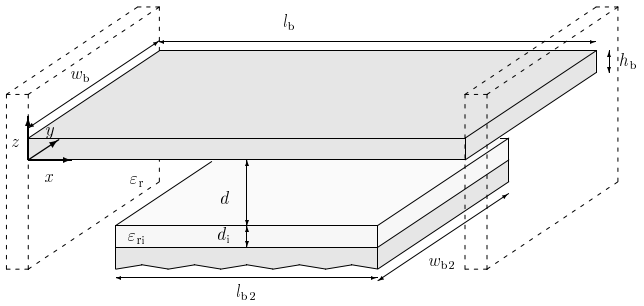

Figure 1: Simplified structure of a doubly supported capacitive RF Switch.

2.1 Beam Deflection

When an extrinsic force is applied to a beam, the beam deflection is given by [3], [4]

$$\frac{\partial^2}{\partial x^2}\left(\tilde{E} I_\mathrm{y} \frac{\partial^2 z}{\partial x^2}\right) + h_\mathrm{b} w_\mathrm{b} \frac{\partial}{\partial x}\left(S \frac{\partial z}{\partial x}\right) = q(x,z), \qquad (1)$$

where I_y is the second area momentum, q is the load density, z is the deflection and S is the stress in the beam. Beam width and height are denoted with w_b and h_b, respectively. For narrow beams, Young's modulus E can be used instead of the effective value $\tilde{E}$, which in this case is specified to be the plate modulus $\tilde{E} = E/(1-\nu^2)$, where ν is Poisson's ratio. For a beam with a rectangular cross-section, the second area momentum is given by $I_\mathrm{y} = h_\mathrm{b}^3 w_\mathrm{b}/12$ [5].
If a uniform and homogenous structure and a uniform stress is assumed along the beam length, Eq. (1) reduces to

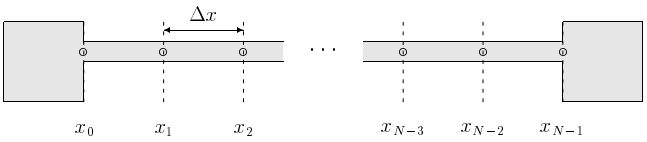

Figure 2: Beam discretization into N sections. Each section has length Δx.

$$\tilde{E} I_{\mathrm{y}} \frac{\partial^4 z}{\partial x^4} + h_{\mathrm{b}} w_{\mathrm{b}} S \frac{\partial^2 z}{\partial x^2} = q(x, z). \tag{2}$$

According to the finite-difference procedure, the beam is discretized into N sections as presented in Fig. 2. The continuous displacement $z(x)$ is replaced with N discrete displacements $z(x_n)$ denoted with z_n. Now, the second- and fourth-order spatial derivatives in Eq. (2) can be expressed in a discretized form

$$\frac{\partial^4 z}{\partial x^4} = \frac{M_2 z_{n-2} + M_1 z_{n-1} + P_0 z_n + P_1 z_{n+1} + P_2 z_{n+2}}{(\Delta x)^4}, \tag{3}$$

$$\frac{\partial^2 z}{\partial x^2} = \frac{z_{n-1} - 2 z_n + z_{n+1}}{(\Delta x)^2}, \tag{4}$$

where coefficients M_2, M_1, P_0, P_1 and P_2 depend on the boundary conditions and on the element location in the beam. For a doubly supported beam, the boundary conditions set the deflection and its first spatial derivative to zero at the beam ends ($z(0) = z(l_{\mathrm{b}}) = 0$, $z'(0) = z'(l_{\mathrm{b}}) = 0$); the resulting coefficients are shown in Table 1. There is no need to define coefficients for the second-order term, since the first and the last element are not generated due to their trivial solution ($z_0 = z_{N-1} = 0$).

Table 1: Coefficients for beam elements.

Element number	M_2	M_1	P_0	P_1	P_2
1	0	0	0	0	0
2	0	-4	7	-4	1
3 ... N-2	1	-4	6	-4	1
N-1	1	-4	7	-4	0
N	0	0	0	0	0

The stress can be divided into two parts, the static residual stress S_{R} which is caused when the membrane is processed, and the elongation stress which is caused by the beam deflection. The total stress is defined to be [5]

$$S = S_{\mathrm{R}} + \frac{\tilde{E}}{2 l_{\mathrm{b}}} \sum_{n=0}^{N-1} W_n \frac{(z_{n+1} - z_{n-1})^2}{4 \Delta x}, \tag{5}$$

where W_n is a weighting coefficient for extended trapezoidal rule numerical integration.

2.1.1 Electrical equivalent circuit

The equivalent circuit for beam deflection is constructed using fundamental circuit blocks [1] for force and displacement. The spring force for each discrete section is generated with a current source (VCCS) connected between velocity nodes. The source is controlled with 5 displacements; z_{n-2}, z_{n-1}, z_n, z_{n+1}, and z_{n+2} as well as the elongation voltage u_{E}. This implements the spatial derivative terms from Eq. (2). The displacement voltage z_n ($v_n = \partial z_n / \partial t$) is generated using a current source in parallel with a capacitor. Each section generates an elongation current source between ground and elongation node `nE` to implement Eq. (5). A 1 Ω resistor is used to generate the elongation voltage u_{E} which represents the total elongation.

2.2 Capacitance Model

An electromechanical transducer is used to generate the electrostatic force according to the the voltage across the upper and lower membrane, i.e., the actuation voltage U and beam displacement [1]. The electrostatic force acting on the capacitor surfaces is

$$F_{\mathrm{el}} = \frac{U^2}{2} \frac{\partial C}{\partial h}, \tag{6}$$

where $h = d + z$ is the dynamic gap height. The transducer also includes the corresponding capacitance. Since the beam deflection is known at N discrete points, the gap between the plates is also known at discrete points. At each discrete point, a parallel-plate capacitor with length Δx and width w_{b} is assumed. For a parallel-plate capacitor with an isolating layer having permittivity $\varepsilon_{\mathrm{ri}}$ and thickness d_{i}, the capacitance is given by

$$C = \frac{\varepsilon_{\mathrm{ri}} \varepsilon_0 A}{\frac{\varepsilon_{\mathrm{ri}}}{\varepsilon_{\mathrm{r}}} h + d_{\mathrm{i}}}, \tag{7}$$

where $A = \Delta x w_{\mathrm{b}}$ is the plate area and ε_{r} is the gas permittivity.

The surface roughness of the isolating layer is taken into account by assuming a linear behaviour for the surface, which means that the rough surface blisters are assumed to be triangles above a smooth surface. This is similar to having a smooth surface slanted from $-\frac{B}{2}$ to $\frac{B}{2}$ as shown in Fig. 3, where B is the surface height distribution. For a small change in the x-direction, the differential capacitance can now be written

$$\Delta C = \frac{\varepsilon_{\mathrm{ri}} \varepsilon_0 A \Delta x}{\frac{\varepsilon_{\mathrm{ri}}}{\varepsilon_{\mathrm{r}}} (h - \Delta h) + d_{\mathrm{i}} + \Delta h}, \qquad h > \frac{B}{2}. \tag{8}$$

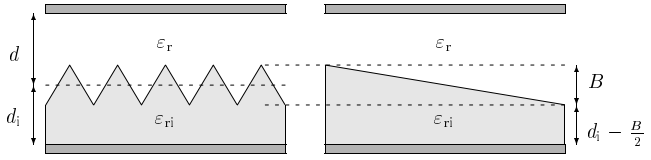

Figure 3: Modelling roughness with a slanted surface.

Since the surface is linearly slanted, $\Delta h = Bx$. When $h > \frac{B}{2}$, there is no contact and the capacitance is calculated by integrating over the normalized length x. The result is given by

$$C(h) = \frac{\varepsilon_{ri}\varepsilon_0 A}{2B_2} \ln\left(\frac{\frac{\varepsilon_{ri}}{\varepsilon_r}h + d_i + B_2}{\frac{\varepsilon_{ri}}{\varepsilon_r}h + d_i - B_2}\right), \qquad h > \frac{B}{2}, \quad (9)$$

where $B_2 = B(1 - \varepsilon_{ri}/\varepsilon_r)/2$. At contact ($h \leq \frac{B}{2}$), the following second order polynomial function is used

$$\tilde{C}(h) = K_0 + K_1 h + K_2 h^2, \qquad h \leq \frac{B}{2}. \quad (10)$$

Coefficients K_0, K_1, and K_2 are calculated by forcing functions $C(h)$ and $\tilde{C}(h)$ as well as their first and second derivatives to be continuous. This yields

$$K_0 = C(B/2) - \frac{B}{2}C'(B/2) + \frac{B^2}{8}C''(B/2), \quad (11)$$

$$K_1 = C'(B/2) - \frac{B}{2}C''(B/2), \quad (12)$$

$$K_2 = \frac{1}{2}C''(B/2). \quad (13)$$

The electromechanical transducer is implemented using a VCCS connected between velocity nodes along with a capacitor between electrical nodes [1]. Both components are controlled by the electrical voltage and the displacement voltage.

2.3 Mechanical Contact

The mechanical contact model is based on collision between two rough surfaces containing spherical caps as presented by Greenwood [6]. The rough surface is assumed to be composed of several caps with different heights according to the height probability distribution function. The mechanical contact is modelled using a VCCS which implements the contact force.

2.4 Complete Model

The model is based on the switch structure shown in Fig. 1. The beam profile is assumed to be uniform. The complete model is constructed by dividing the beam structure into N sections. The internal structure of the capacitive switch model is shown in Fig. 4. Each section includes three APLAC [7] micromechanical library components. A model for beam deflection (`BE`) is controlled by the displacements of two preceding and two following sections, see Eqs. (3) and (4). A transducer (`NTR`) and mechanical contact (`NC`) complete the model for Nth part of the switch structure. Each section has three nodes, velocity node `nv[i]`, displacement node `nz[i]`, and the elongation node `nE`.

A model for symmetrical switch structure has also been implemented making it possible to model only one half of the beam. The other end's boundary conditions must be changed ($z'(l_b/2) = z^{(3)}(l_b/2) = 0$) and boundary effects must be included also in the second-order term. Also the transducer capacitor values and elongation resistor value must be multiplied by two.

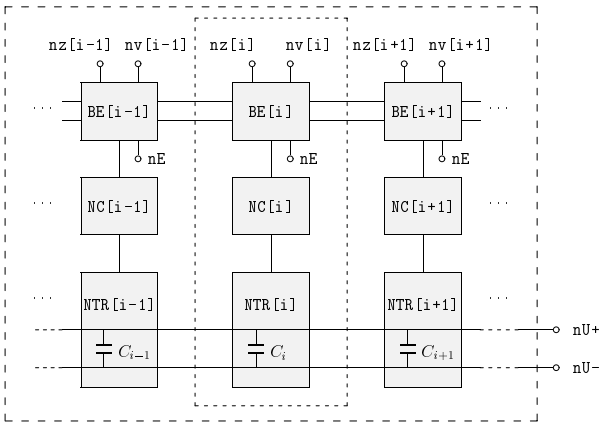

Figure 4: Internal structure of capacitive switch model. `BeamElements` (`BE`) are mutually connected with four adjacent elements. `NormalContacts` (`NC`) and `NormalTransducers` (`NTR`) are not directly controlled by adjacent sections. Transducer capacitors are connected in parallel.

3 MODEL VERIFICATION

Several MEMS switchable capacitors have been designed and fabricated. The structural material was chosen to be gold due to its high conductivity and due to fabrication issues. Since no suitable MEMS process was available, a new process was developed at Tronic's Microsystems, France. The process uses gold to form both a bottom electrode (metal 1) as well as the suspended electrode (metal 2). A silicon nitride dielectric layer isolates the suspended electrode from the bottom electrode in case of a pull-in. Polymer is used as a sacrificial material and it is planarized before the deposition of the metal 2. In addition, the process contains a third metal layer which is used as structural material in anchoring and to form coils.

Measured CV characteristics of the switch shown in Fig. 5 are compared to the simulation results in Fig. 6.

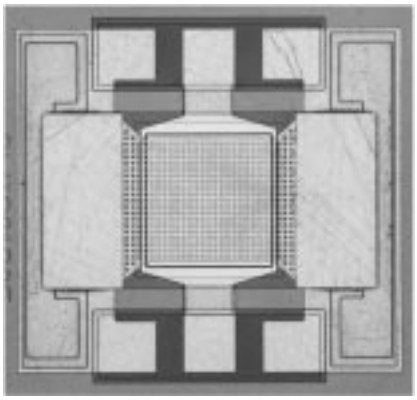

Figure 5: Top view of the manufactured capacitive RF switch.

The dimensions of the measured switch are shown in Table 2. In simulations, the switch structure was divided into 100 sections as presented earlier. Transient analysis with a very low frequency ramped pulse was utilized to avoid multiple DC solution caused by the component's hysteretic behaviour. A constant capacitance of 600 fF was added to model the stray capacitance, and the surface roughness in the isolating layer was modified. Static residual stress was set to 20MPa.

Table 2: Dimensions (see Fig. 1) in μm for the switch used in verifying the simulation results.

Beam length	l_b	332
Beam width	w_b	236
Beam height	h_b	0.5
Lower electrode length	l_b2	240
Static gap height	d	0.5
Isolating layer height	d_i	0.1
Surface roughness	B	0.03

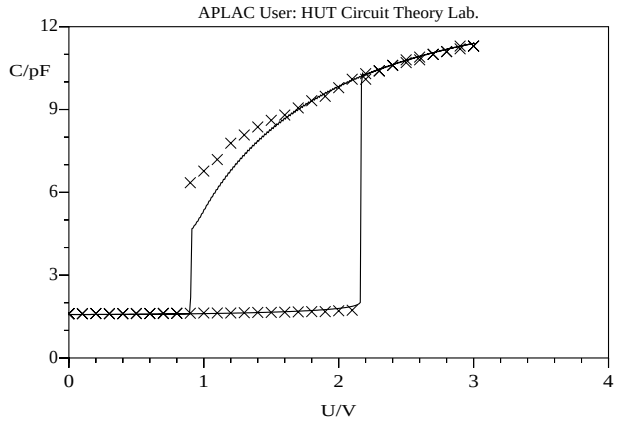

Figure 6: Measured (×) and simulated (——) CV characteristics for capacitive RF switch.

4 CONCLUSIONS

A static simulation model for a doubly supported capacitive MEMS RF switch was presented. The model is based on electrical-equivalent macro models for beam deflection, electromechanical transducer, and mechanical contact. The fourth-order differential equation for beam deflection is solved using finite differences. The gap capacitance is modelled using a parallel-plate approximation taking into account the permittivity of the isolating layer and the surface roughness. Comparison with measurement results show that the model correctly reproduces the CV characteristics, including the performance at contact. That is due to the increased area in contact when voltage is increased and also to the plate being able to press the isolating layer.

ACKNOWLEDGEMENT

The tunable RF capacitors were fabricated by Christian Pisella, Stéphane Renard, and Marjorie Trzmiel of Tronic's Microsystems, Grenoble, France.

REFERENCES

[1] T. Veijola, "Nonlinear Circuit Simulation of MEMS Components: Controlled Current Source Approach," *Proceedings of the 15th European Conference on Circuit Theory and Design*, (Espoo), pp. 377–380, August 2001.

[2] J.-M. Huang, K. M. Liew, C. H. Wong, S. Rajendran, M. J. Tan, and A. Q. Liu, "Mechanical Design and Optimization of Capacitive Micromachined Switch," *Sensors and Actuators A*, vol. 93, pp. 273–285, 2001.

[3] E. S. Hung and S. D. Senturia, "Generating Efficient Dynamical Models for Microelectromechanical Systems from a Few Finite-Element Simulation Runs," *Journal of Microelectromechanical Systems*, vol. 8, pp. 280–289, September 1999.

[4] R. H. MacNeal, "The Solution of Elastic Plate Problem by Electrical Analogies," *Journal of Applied Mechanics*, pp. 59–67, March 1951.

[5] R. P. van Kampen, *Bulk-Micromachinend Capacitive Servo-Accelerometer.* PhD thesis, Technical University of Delft, Delft, September 1995.

[6] J. A. Greenwood and J. P. B. Williamsson, "Contact of Nominally Flat Surfaces," *Proc. R. Soc. A.*, vol. 295, pp. 300–319, 1966.

[7] M. Valtonen *et al.*, "APLAC - Object-Oriented Circuit Simulator and Design Tool," *Low-Power HF Microelectronics - a Unified Approach* (G. Machado, ed.), ch. 9, IEE Circuits and Systems Series 8, IEE London, 1996.